[American Journal of Science, Vol. 301, January, 2001, P. 34–59]

MODELING MULTIPHASE NON-ISOTHERMAL FLUID FLOW AND REACTIVE GEOCHEMICAL TRANSPORT IN VARIABLY SATURATED FRACTURED ROCKS: 2. APPLICATIONS TO SUPERGENE COPPER ENRICHMENT AND HYDROTHERMAL FLOWS

TIANFU XU*, ERIC SONNENTHAL*, NICOLAS SPYCHER*, KARSTEN PRUESS*, GEORGE BRIMHALL**, and JOHN APPS*

ABSTRACT. Reactive fluid flow and geochemical transport in unsaturated fractured rocks has been of increasing interest to investigators in the areas of geo- and environmental- sciences. To test geochemical hypotheses based on petrologic observation and to predict geochemical reactions that occur through a complex dynamic interplay of physical and chemical processes, we use the methods presented in a companion paper (part 1, this issue p. 16–33) to investigate two problems: (1) supergene copper enrichment in unsaturated-saturated media and (2) predicted effects of thermohydrology on geochemistry during the Drift Scale Heater Test at the Yucca Mountain potential nuclear waste repository, Nevada. Through these two examples we address the importance of the following issues on geochemical processes: (1) participation of gas phase in transport and reaction, (2) interactions between fractures and rock matrix for water and chemical constituents, (3) heat effects on fluid flow and reaction properties and processes. In the supergene enrichment system, oxygen gas diffusion from the land surface through fractured rock promotes the alteration of the primary sulfide minerals and the subsequent deposition of secondary minerals. Modeling of the large-scale heater test shows effects of fracture-matrix interaction, heat-driven vaporizing fluid flow, and CO_2 degassing on mineral alteration patterns. The two examples also serve as a demonstration of our methods for reactive transport in variably saturated fractured rocks.

INTRODUCTION

Reactive fluid flow and geochemical transport in unsaturated fractured rocks have been of increasing interested to investigators in the areas of geo- and environmental-sciences such as mineral deposits, contaminant transport, groundwater quality, waste disposal, acid mine drainage remediation, sedimentary diagenesis, and fluid-rock interactions in hydrothermal systems. This is a challenging issue because of the complexity of multiphase fluid flow, water-gas-rock and fracture-matrix interaction mechanisms, and difficulties dealing with physical and chemical heterogeneities and the strong non-linearities in the governing equations. For oxidized sulfide ore deposits, microscopic and petrologic studies based on 3-dimensional field mapping offer unique evidence as to the present state of surficial geochemical processes, mineral distribution, and controlling geological, hydrological, tectonic, and climatic factors (Brimhall, Alpers, and Cunningham, 1985; Ague and Brimhall, 1989). In fact, for almost a century supergene leaching and enrichment have been at the core of understanding redox processes at the paleo-ground water table. Geochronological methods cast such hydro-chemical systems in a temporal frame of reference so that an assortment of known deposits may be related in both a relative and absolute sequence of progressive geochemical states.

The scientific relevance of numerical modeling of irreversible natural phenomena depends upon the character of the systems being modeled: natural or anthropogenic. In natural phenomena, the geological relevance of modeling is in hypothesis

*Earth Sciences Division, Lawrence Berkeley National Laboratory, University of California, Berkeley, California 94720.

**Department of Geology and Geophysics, University of California at Berkeley.

testing, not in prediction as the natural processes and geochemical systems are far too complicated to predict anything approaching reality in 3-dimensions at the present time. What is important, however, is in constraining numerical models with boundary and initial conditions derived from integrated observational studies which describe the system in a quantitative petrologic and geochemical manner such that specific, well-posed questions can be answered by numerical results which abstract only the essential features in a vastly simplified domain compared to the realities of nature. It is in this simplification of nature that the real strength of numerical modeling resides. If modeling can find an unambiguous answer to a simple well posed question, then something can be learned. However, the only rigorous test of numerical results is by comparison with known patterns, sequences, and processes from natural systems that are plentiful, although they are usually qualitative rather than quantitative in terms of mineral abundances. In contrast, in anthropogenic systems such as nuclear waste repositories, the scientific relevance of modeling must be in prediction, as few alternatives exist. Similarly, the test of the numerical predictive capabilities must reside only in confirmation by independent methods. Hence, experimental design and validation in natural and anthropogenic systems differ markedly.

It is well-known from past studies (Ague and Brimhall, 1989) that in unsaturated geologic media, the presence of gases has a strong influence on hydrogeochemical evolution which occurs through a complex interplay of multi-phase fluid flow and chemical transport processes. The oxygen consumed during pyrite oxidation in unsaturated media is mainly supplied by gaseous oxygen diffusive transport in the gas-filled portion of the pore space from the land surface.

For unsaturated fractured rocks, global fluid flow and transport of aqueous and gaseous species may occur primarily through a network of interconnected fractures, while chemical species may penetrate into tight matrix blocks primarily through diffusive transport in gas and liquid phases. Depending on the spatial scale of interest, the "kinetics" of water-gas-rock interaction may involve not just "true" chemical kinetics but may be affected by small-scale slow matrix diffusive transport processes. There is evidence from field sites such as the potential high-level nuclear waste disposal site at Yucca Mountain, Nevada (Pruess, 1999) that water can flow rapidly through unsaturated fractured rocks. This kind of flow can occur only in the fracture network, not in matrix rocks of low intrinsic permeability. Changes in chemical concentrations in the fracture fluids could take a long time to propagate to the interior of rock matrix. This is proved by geochemical studies. For example, DePaolo (1999) found significant differences in the isotropic ratios of certain pairs of elements between the fractures and rock matrix. Thordarson (1965) reported on water sampling and hydrogeologic studies at Rainier Mesa, Nevada Test Site, where an unsaturated zone of approx 500 m thickness occurs in fractured tuffs. He noted that the chemical composition of water samples extracted from the rock matrix was considerably different from that of waters sampled in the fractures. The mineralogy of the rock matrix may also be considerably different from that of the fractures, and the reactivity of rock matrix minerals may be different near the fracture walls as compared to the interior of the matrix blocks.

Methods for modeling geochemical reactions in this complex interplay of physical and chemical transport processes are described in a companion paper (Xu and Pruess, this issue, p. 16–33). Our model employs a sequential solution approach and has three important features: (1) gas phase is active for multiphase fluid flow, mass transport, and chemical reactions; (2) the model is not only used for porous media but also well suited for reactive flow and transport in heterogeneous and fractured rocks; and (3) non-isothermal effects are considered, which include boiling and condensation of water and temperature-dependence of thermophysical properties such as fluid density and viscosity and chemical properties such as thermodynamic and kinetic data.

The first geochemical system investigated is supergene copper enrichment (SCE), which involves the oxidative weathering of pyrite (FeS_2) and chalcopyrite ($CuFeS_2$) with subsequent formation of enriched copper deposits under reducing conditions attained at the ground water table and below. Oxygen gas diffusion plays a dominant role in the SCE processes. This study is intended to provide a better understanding of the coupled processes of transport of aqueous and gaseous chemical species, sulfide mineral oxidation, acidification, and subsequent intense alteration of primary minerals and reprecipitation of secondary minerals.

We then present a model of geochemical changes due to hydrothermal processes that are induced by emplacement of a strong heat source in unsaturated fractured volcanic tuffs. The large permeability contrast between the matrix (10^{-17} m^2) and the fracture system (10^{-13} m^2) results in very different liquid and vapor flow in the two media: (1) boiling in the matrix with vapor discharge into the fractures and (2) condensation in cooler portions of the fractures followed by water imbibition into the matrix. CO_2 is volatilized from the matrix pore water and discharged into the fractures. The changes in CO_2 partial pressure control the pH, water chemistry, and mineral dissolution and precipitation patterns.

SUPERGENE COPPER ENRICHMENT

Supergene copper enrichment (SCE) involves hydrochemical differentiation by near-surface weathering processes in which water transports metals from a source region or leached zone (Brimhall, Alpers, and Cunningham, 1985; Brimhall and Dietrich, 1987; Ague and Brimhall, 1989) to a locus of an enrichment blanket zone where these ions are reprecipitated as secondary ore compounds conserving mass (fig. 1). The schematic system shown in figure 1 captures, in a simplified manner, conditions of desertification in Northern Chile that led to oxidation and chemical enrichment of copper deposits at certain times in the past (of order 15 Ma) when downward movements in the ground water table exposed sulfides to unsaturated conditions (Brimhall, Alpers, and Cunningham, 1985; Brimhall and Dietrich, 1987; Alpers and Brimhall, 1988; Ague and Brimhall, 1989).

Oxidative weathering of pyrite (FeS_2) and chalcopyrite ($CuFeS_2$) causes acidification and mobilization of metals in the oxidizing zone and intense alteration of primary minerals, with subsequent formation of enriched secondary copper bearing sulfide mineral deposits (enrichment blanket) in the reducing conditions below the water

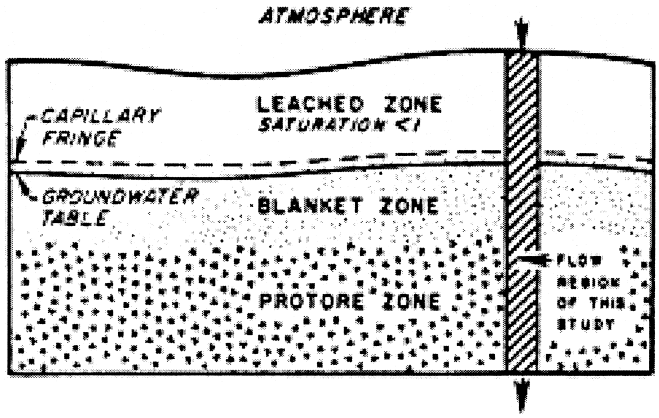

Fig. 1. A schematic representation of a supergene copper enrichment system according to Ague and Brimhall (1989).

table. Such oxidative weathering driven processes have produced some of the world's largest copper deposits (Ague and Brimhall, 1989). The present investigation on geochemical transport in SCE systems is not specific to any field site, but the geochemistry for this work was based on field and laboratory studies of SCE systems as carried out by Brimhall, Alpers, and Cunningham (1985) and Ague and Brimhall (1989). The coupled modeling study is intended to provide a better understanding of the complex interplay of oxygen diffusion, sulfide mineral oxidation, subsequent intense alteration of primary minerals, and reprecipitation of secondary minerals. The SCE processes typically took place in a fractured porous medium such as El Salvador, Chile (Mote and Brimhall, 1999). To gain better insight into the processes involved, we first consider a problem in a one-dimensional unsaturated-saturated porous medium flow. A simple porous medium description may be applicable in regions with highly fractured rocks. Then we present the case of SCE processes in a variably saturated fractured rock system using the "multiple interacting continua" (MINC) method.

One-dimensional porous medium.—A one-dimensional (1-D) supergene copper enrichment (SCE) system has been simulated and analyzed by Ague and Brimhall (1989). We extended the processes considered in the previous work by adding oxygen gas transport, which is coupled with SCE geochemistry in a dynamic fashion. In addition, we use a step change of infiltration rate and water table elevation for this 1-D homogeneous medium study. The model system is shown in figure 2. Oxygen is supplied to a protore containing pyrite and chalcopyrite (table 1) as a dissolved species in infiltrating rainwater, as well as by gaseous transport from the land surface boundary. A vertical column of 40 m thickness is used, which is discretized into 20 grid blocks with a constant spacing of 2 m. A medium permeability of 1.0×10^{-12} m^2 is used. Hydrodynamic dispersion is neglected, which has been discussed in a companion

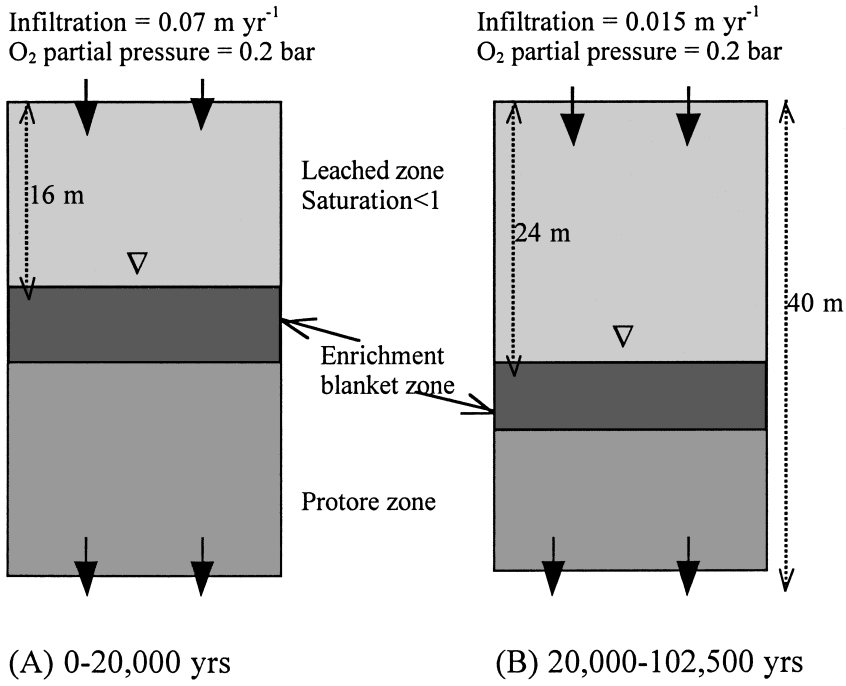

Fig. 2. Problem setup of a one-dimensional supergene copper enrichment system.

TABLE 1

Initial protore mineral volume fractions (V_f) and possible secondary mineral phases (V_f = 0.0) considered in the supergene copper enrichment problem. Kinetic data of primary minerals are based on Ague and Brimhall (1989) and Gérard and others (1997)

Mineral	Composition	Volume fraction, V_f	Rate constant at 25°C (mol $m^{-2}s^{-1}$)	Surface area (m^2 dm^{-3} medium)
Primary:				
pyrite	FeS_2	0.090	4.0×10^{-11}	0.0587
chalcopyrite	$CuFeS_2$	0.045	4.0×10^{-11}	0.0587
magnetite	Fe_3O_4	0.045	2.0×10^{-11}	0.0787
k-feldspar	$KAlSi_3O_8$	0.180	3.1×10^{-12}	0.2710
albite	$NaAlSi_3O_8$	0.090	3.1×10^{-12}	0.1360
anorthite	$CaAl_2Si_2O_8$	0.090	1.5×10^{-12}	0.1420
annite	$KFe_3AlSi_3O_{10}(OH)_2$	0.045	2.4×10^{-14}	0.0587
muscovite	$KAl_3Si_3O_{10}(OH)_2$	0.090	2.4×10^{-14}	0.0123
quartz	SiO_2	0.180	4.3×10^{-14}	0.0850
anhydrite	$CaSO_4$	0.045	1.5×10^{-12}	0.0510
		total=0.9		
		porosity=0.1		
Secondary:				
covellite	CuS	0.0	2.0×10^{-10}	0.1
chalcocite	Cu_2S	0.0	2.0×10^{-10}	0.1
bornite	Cu_5FeS_4	0.0	2.0×10^{-10}	0.1
goethite	FeOOH	0.0	2.0×10^{-10}	0.1
hematite	Fe_2O_3	0.0	2.0×10^{-10}	0.1
kaolinite	$Al_2Si_2O_5(OH)_4$	0.0	2.0×10^{-10}	0.1
alunite	$KAl_3(OH)_6(SO_4)_2$	0.0	2.0×10^{-10}	0.1
amorphous silica	SiO_2	0.0	2.0×10^{-10}	0.1

paper (Xu and Pruess, this issue, p. 16–33) Oxygen diffusion coefficients are 2.20×10^{-5} m^2s^{-1} for gas and 1.0×10^{-10} m^2s^{-1} for aqueous phase. Tortuosity is calculated from eq (4) presented in Xu and Pruess (first of this two-part paper, this issue, p. 16–33). Two steady-state water flow regimes are assumed (see fig. 3). In the first period of 20,000 yrs, a net infiltration of 0.07 m yr^{-1} is assumed, and the water table is located at a depth of 16 m. After 20,000 yrs, the infiltration is assumed to reduce to 0.015 m yr^{-1}, and the water table moves down to a depth of 24 m. Strictly speaking, infiltration decrease and water table drop is achieved gradually but is assumed here to be instantaneous for simplicity. Over extended time periods, changes in porosity and permeability due to mineral dissolution and precipitation can cause changes in fluid flow. However, by neglecting such changes, a "quasi-stationary state" (QSS; Lichtner, 1988) is obtained for the reactive system, which provides a tremendous simplification of the computational problem and makes it possible to consider the difficult redox geochemistry in great detail. Although we do not allow porosity change to affect fluid flow, we monitor it during the simulation based on changes in mineral abundances.

The geochemical transport simulation considers unsaturated-saturated liquid phase flow and diffusive supply of oxygen to the protore. The 1-D column modeled is initially filled entirely with a protore mineral assemblage as listed in table 1. The dissolution of the primary minerals is considered to be kinetically-controlled. The kinetic rate law used is given in eq (1) of Xu and Pruess (this issue, p. 16–33). The kinetic rate constants and specific surface areas used are also given in table 1. Precipitation of secondary minerals (table 1 with initial $V_f = 0$ where V_f is mineral volume fraction) is represented using the same expression as dissolution. However,

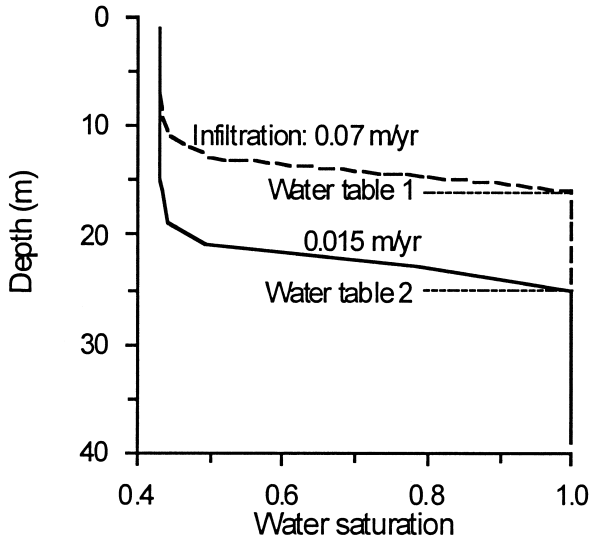

Fig. 3. Steady-state water saturation distribution along the 1-D unsaturated-saturated homogeneous medium.

precipitation may be different in several aspects, including sequence of nucleation, Ostwald ripening and crystal growth processes, and the reactive surface areas (Plummer, Wigley, and Parkhurst, 1978; Steefel and van Capellen, 1990). To simplify the description of precipitation kinetics, in the present study all secondary minerals are assigned the same kinetic constant (2.0×10^{-10} mol $m^{-2}s^{-1}$) and reactive surface areas (0.1 m^2 per dm^3 bulk medium). Because the rate constants assumed for precipitation reactions are larger than those for dissolution of primary minerals, formation of secondary minerals occurs effectively at conditions close to local equilibrium. The kinetic rate of sulfide mineral oxidation can be strongly influenced by catalytic effects of bacteria (Singer and Stumm, 1970; Olson, 1991; Nordstrom and Alpers, 1997), which are not considered in the present study. Estimates of field oxidation rate cover a wide range of values (Nordstrom and Alpers, 1997). The rate determining process is often transport of oxygen or other reactants to the reaction site. This is the process we are investigating in this work. Heat generation by pyrite oxidation may change temperature, but this effect is not considered in our simulations. Calculations are carried out at a constant temperature of 25°C. Thermodynamic data used in the simulations were taken from the EQ3/6 V7.2b database (Wolery, 1992) which were derived using SUPCRT92 (Johnson, Oelkers, and Helgeson, 1992). The chemical formulae and equilibrium constants of the primary minerals are given in table 2, and those for secondary minerals in table 3.

Oxygen is treated as an ideal gas, and its interaction with the aqueous solution is assumed at equilibrium. The oxygen partial pressure at the land surface boundary is assumed to be constant at 0.2 bar. A dilute oxidizing water equilibrated with an oxygen partial pressure of 0.2 bar is initially placed in the unsaturated zone, while a reducing water is assumed for the saturated zone. The infiltration water composition is the same as the initial unsaturated water. Aqueous species considered are listed in table 4. The aqueous complexation is assumed at equilibrium, even though some aqueous redox pairs such as sulfite and sulfide species may not be at equilibrium (Stumm and Morgan, 1981). Whether a particular reaction should be described as governed by the local equilibrium approximation (LEA) or by kinetic rates depends not only on the reaction

TABLE 2

Chemical reactions for the primary minerals

Mineral	Reactions equation	log K (25°C)
Pyrite	$FeS_2 + H_2O + 3.5O_2(aq) = 2SO_4^{2-} + Fe^{2+} + 2H^+$	217.4
Chalcopyrite	$CuFeS_2 + 4O_2(aq) = 2SO_4^{2-} + Fe^{2+} + Cu^{2+}$	244.07
Magnetite	$Fe_3O_4 + 8H^+ = Fe^{2+} + 2Fe^{3+} + 4H_2O$	10.4724
K-feldspar	$KAlSi_3O_8 + 4H^+ = K^+ + Al^{3+} + 3\ SiO_2(aq) + 2H_2O$	-0.2753
Albite	$NaAlSi_3O_8 + 4H^+ = Na^+ + Al^{3+} + 3\ SiO_2(aq) + 2H_2O$	2.7645
Anorthite	$CaAl_2Si_2O_8 + 8H^+ = Ca^{2+} + 2Al^{3+} + 2\ SiO_2(aq) + 4H_2O$	26.5780
Annite	$KFe_3AlSi_3O_{10}(OH)_2 + 10H^+ = K^+ + 3Fe^{2+} + Al^{3+} + 3\ SiO_2(aq) + 6H_2O$	29.4693
Muscovite	$KAl_3Si_3O_{10}(OH)_2 + 10H^+ = K^+ + 3Al^{3+} + 3\ SiO_2(aq) + 6H_2O$	13.5858
Quartz	$SiO_2 = SiO_2(aq)$	-3.9993
Anhydrite	$CaSO_4 = Ca^{2+} + SO_4^{2-}$	-4.3064

itself but also on the rates of hydrodynamic transport processes (Domenico and Schwarz, 1990). The LEA is applicable when the characteristic time for transport of reactants is longer than the time required to reach chemical equilibrium. In the present simulations for reactive geochemical transport, the choice of equilibrium depends mainly on kinetic rate, infiltration rate, oxygen availability, and space discretization.

As expected, the 1-D porous medium simulation shows that in the unsaturated zone pyrite and chalcopyrite are both oxidized and decrease in abundance due to dissolution (fig. 4A). It is well-known that in nature complete dissolution is relatively uncommon. Instead, goethite, hematite (or jarosite) replace primary sulfide minerals which undergo oxidation in the unsaturated zone. We do not treat in this study the transformation mechanisms but only the bulk dissolution and precipitation processes predicted by irreversible thermodynamic simulation and reaction kinetics. As aqueous phase oxygen is depleted through reaction with pyrite and chalcopyrite, it is replenished by dissolution from the gas phase and by diffusive transport from the atmospheric boundary at the land surface (fig. 4C). The pH decreases downward in the unsaturated zone (fig. 4D) due to sulfide mineral oxidative dissolution. The total dissolved chemical concentration increases downward. When the aqueous solution reaches the reducing saturated zone, the secondary copper-bearing minerals chalcocite and covellite are precipitated (fig. 4B), forming the enrichment blanket immediately below the water table. In addition, goethite precipitates in the unsaturated zone. At the same time, magnetite, k-feldspar, albite, anorthite, annite, and muscovite

TABLE 3

The chemical reactions for the secondary minerals

Mineral	Reaction equation	log K (25°C)
Covellite	$CuS + H^+ = Cu^{2+} + HS^-$	-22.8310
Chalcocite	$Cu_2S + H^+ = 2Cu^+ + HS^-$	-34.7342
Bornite	$Cu_5FeS_4 + 4H^+ = Cu^{2+} + 4Cu^+ + Fe^{2+} + 4HS^-$	-102.44
Goethite	$FeOOH + 3H^+ = Fe^{3+} + 2H_2O$	-0.283
Hematite	$Fe_2O_3 + 6H^+ = 2Fe^{3+} + 3H_2O$	0.1086
Kaolinite	$Al_2Si_2O_5(OH)_4 + 6H^+ = 2Al^{3+} + 2\ SiO_2(aq) + 5H_2O$	6.8101
Alunite	$KAl_3(OH)_6(SO_4)_2 + 6H^+ = K^+ + 3Al^{3+} + 2SO_4^{--} + 6H_2O$	-0.3479
Amorphous silica	$SiO_2 = SiO_2(aq)$	-2.7136

TABLE 4

Aqueous species considered in the supergene copper enrichment simulations. Secondary species (or aqueous complexes) can be expressed in terms of the primary species

Primary species:	Secondary species:		
H^+	OH^-	$Al_2(OH)_2^{4+}$	$CaOH^+$
H_2O	HSO_4^-	$Al_3(OH)_4^{5+}$	Cu^+
$O_2(aq)$	$H_2SO_4(aq)$	$HAlO_2(aq)$	$CuOH^+$
SO_4^{2-}	$NaSO_4^-$	AlO_2^-	$CuCl_2(aq)$
Fe^{2+}	KSO_4^-	$FeCl^{2+}$	$CuCl_2^-$
Cu^{2+}	$CaSO_4(aq)$	$FeCl_2^+$	$CuCl_4^{2-}$
Na^+	$FeSO_4(aq)$	$FeOH^+$	$CaCl^+$
K^+	$Fe(SO_4)_2^-$	$FeOH^{2+}$	$KCl(aq)$
Ca^{2+}	$FeSO_4^+$	$Fe(OH)_2^+$	Fe^{3+}
Al^{3+}	$FeCl^+$	$Fe_2(OH)_2^{4+}$	HS^-
$SiO_2(aq)$	$AlSO_4^+$	$Fe(OH)_2(aq)$	$H_2S(aq)$
Cl^-	$Al(SO_4)_2^-$	$Fe(OH)_3(aq)$	$HSiO_3^-$
	$AlOH^{2+}$	$Fe_3(OH)_4^{5+}$	$NaHSiO_3(aq)$
	$Al(OH)_2^+$		

dissolve throughout the column due to a decrease in pH (more results are given in Xu, Pruess, and Brimhall, 1999). Magnetite dissolution creates additional Fe^{2+} and Fe^{3+}. Fe^{3+} also acts as an oxidant, which contributes to pyrite and chalcopyrite oxidation. Dissolution of k-feldspar, albite, anorthite, annite, and muscovite produces Na, K, Ca, Al, and $SiO_2(aq)$. As a result, amorphous silica precipitates throughout the column. Kaolinite (fig. 4B) and alunite precipitation occurs only in the bottom of the saturated zone. There is no quartz dissolution in this system as this mineral is stable in our simulation, as it is in nature.

After the water table drops from 16 to 24 m depth at t = 20,000 yrs, the transition zone or the first enrichment blanket becomes water unsaturated. Gaseous oxygen can access this zone to oxidize the secondary sulfide minerals chalcocite and covellite, which are stable before the water table drop, in addition to the primary protore minerals pyrite and chalcopyrite (fig. 5A). The first enrichment blanket gradually disappears, and a new enrichment zone is formed below the new water table (fig. 5B). The secondary mineral phases forming after the drop of the water table are the same ones as precipitated for the first position of the water table.

The water table drop not only results in aqueous chemical movement but also secondary sulfide mineral migration. The latter is much slower. In this example it takes approx 80,000 yrs to dissolve and reprecipitate the first enrichment blanket. The copper bearing minerals (chalcopyrite, chalcocite, and covellite) migrate downward at an average rate of 1.0×10^{-4} m yr^{-1} (1 mm for 10 yrs). In the first time period (0-20,000 yrs), copper-bearing mineral (only chalcopyrite with 4.5 percent by volume abundance) is dissolved completely after 14,192 yrs and migrates downward at an average rate of 1.127×10^{-3} m yr^{-1} (1.127 mm for 1 yr). The migration in the first time period is about 11 times faster than that in the second period. Considering that the first infiltration rate is 4.667 times greater than the second (0.07 over 0.015 m yr^{-1}), the first migration per unit infiltration is still 2.4 times faster than the second. This is mainly because the copper abundance in the first leaching zone is lower than in

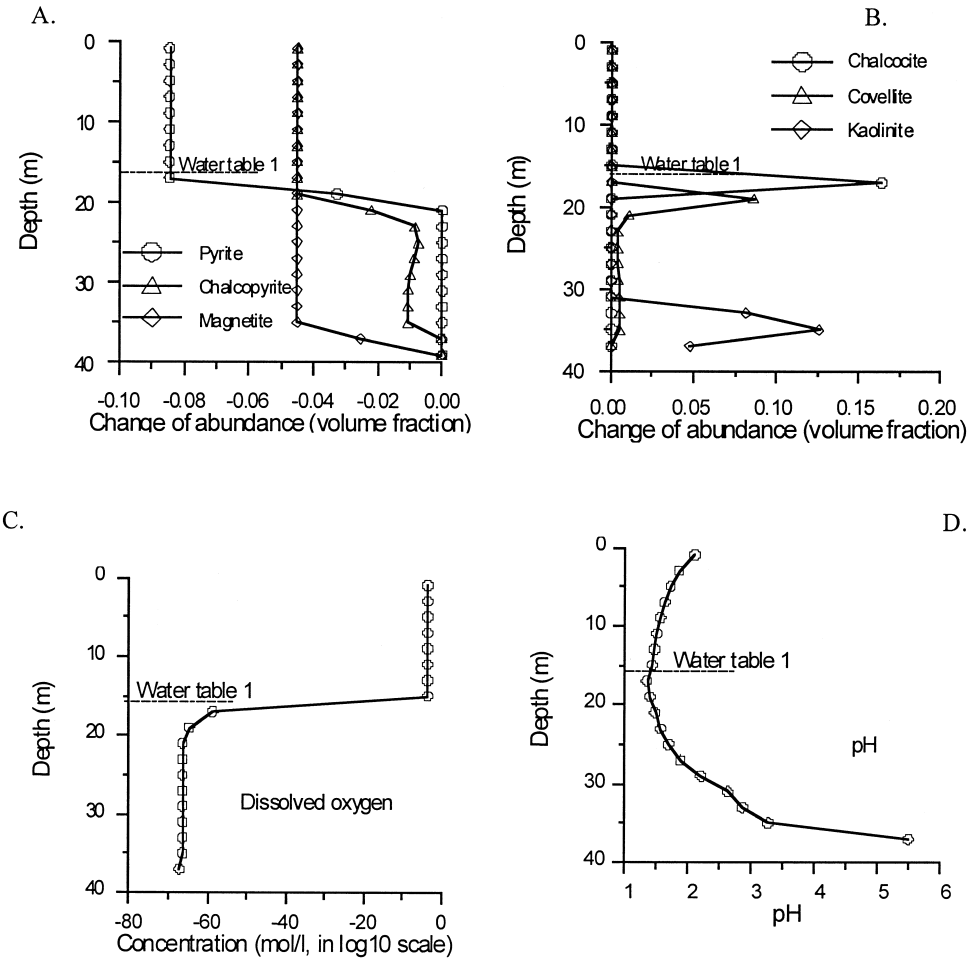

Fig. 4. Change of mineral abundance (A, B; negative values indicate dissolution, and positive indicate precipitation.), dissolved oxygen concentration (C), and pH (D) after 20,000 years.

the second. Therefore, in general the migration rate of the enrichment blanket decreases gradually with depth. The time required to transport the minerals depends on many factors such as kinetic dissolution rates, reactive surface area, atmospheric oxygen partial pressure, medium tortuosity, infiltration rate, and water table depth.

Fractured rock.—The method of "multiple interacting continua" (MINC) is used to resolve "global" flow and diffusion of chemicals in the fractured rock and its interaction with "local" exchange between fracture and matrix rock. This method was developed by Pruess and Narasimhan (1985) for fluid and heat flow in fractured porous media. The extension of the MINC method to reactive geochemical transport is described in detail by Xu and Pruess (this issue, p. 16–33). It is well-known that in the case of reactive chemistry diffusive fluxes may be controlled by reactions occurring near (within millimeters) the fracture walls. The resolution of concentration gradients in matrix blocks is achieved by appropriate subgridding. The MINC concept is based on the notion that changes in fluid pressures and chemical concentrations propagate rapidly through the fracture system, while invading the tight matrix blocks only slowly.

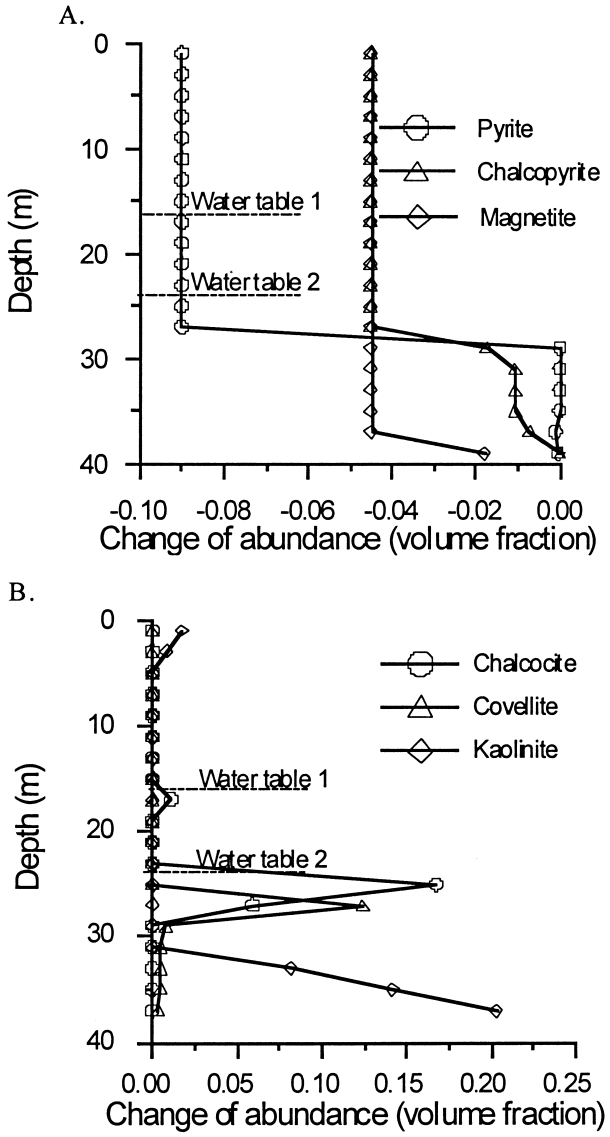

Fig. 5. Change of mineral abundance after 102,500 yrs.

Therefore, changes in matrix conditions will be (locally) controlled by the distance from the fractures and can then be modeled by means of one-dimensional strings of nested grid blocks (fig. 6).

We consider an idealized fractured porous medium with two perpendicular sets of plane, parallel vertical fractures of equal aperture and spacing. Because of symmetry only one column of matrix blocks needs to be modeled. Figure 6 shows an areal view of a rock matrix column surrounded by vertical fractures with a spacing of 0.5 m, with subgridding of the matrix according to the MINC method. Subgrid 1 represents the fracture domain defined to include 50 percent by volume of wall rock. Subgrids 2 through 7 represent the rock matrix. In the vertical direction, a total of 10 grid block

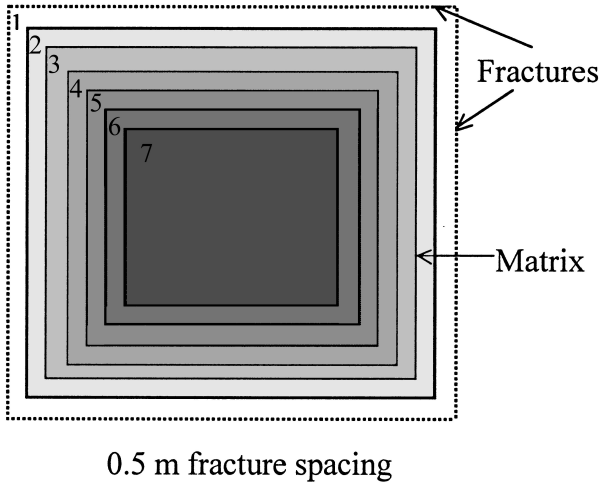

Fig. 6. Subgridding of a rock matrix in the method of "multiple interacting continua" (MINC). The figure represents an areal view of a rock matrix column surrounded by vertical fractures.

zones are used with a spacing of 2 m. A net rainwater infiltration rate of 0.015 my^{-1} over the entire area was applied to the fractures. Water pressure is held constant at 2 bar at the bottom ($z = -20$ m), so that the water table is located at a depth of 10 m. In addition to global water flow and chemical transport in the fracture network, our model considers flow and transport between fractures and matrix as well as vertical matrix-matrix water flow and chemical transport. The steady-state water saturations obtained without chemical reactions are used as initial conditions for the calculation of reactive geochemical transport. Hydrological parameters for the fracture and matrix are listed in table 5. Use of the MINC method also allows us to specify different geochemical properties among subgrids of a matrix block. To take into account that reactive surface areas may decrease from the fractures to the interior of a rock matrix, we assign to each subgrid a reduction factor (1, 0.5, 0.2, 0.06, 0.02, 0.004, and 0.0005 from the fracture to the matrix interior subgrids) for the surface areas of primary minerals given in table 1. The numerical values chosen for reduction factors are quite

Table 5

Hydrological paramenters used for supergene copper enrichment in the fractured rock

Parameter	Matrix	Fracture
Permeability (m^2)	10^{-16}	10^{-12}
Fracture domain volume fraction, v *		0.01
Fracture spacing (m)		0.5
Porosity	0.08	0.5
Relative permeability and capillary pressure (van Genuchten, 1980):		
λ	0.457	0.457
S_{lr}	0.1	0.05
S_{ls}	1.0	1.0
P_0(pa)	2.17×10^5	6.2×10^3

* $v = V_f/(V_f + V_m)$ where V_f and V_m are fracture and matrix domain volumes.

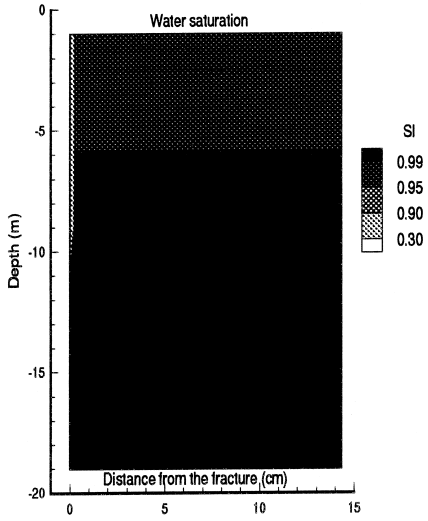

Fig. 7. Water saturation distribution at steady-state in the fractured rock.

artificial and were chosen to represent a general expected trend. The other conditions and parameters are unchanged from the previous 1-D simulation.

The simulation for the fractured rock indicates that the tight rock matrix has strong capillary suction and is almost water saturated (fig. 7), while the fractures in the unsaturated zone have a water saturation of 0.3 (fig. 8). Most pores in the unsaturated fractures are filled with gas phase, which provides an oxygen diffusion path from the land surface. The water entering the fractures at the land surface boundary is imbibed into the rock matrix, reducing flow in the fractures to less than 20 percent of the total

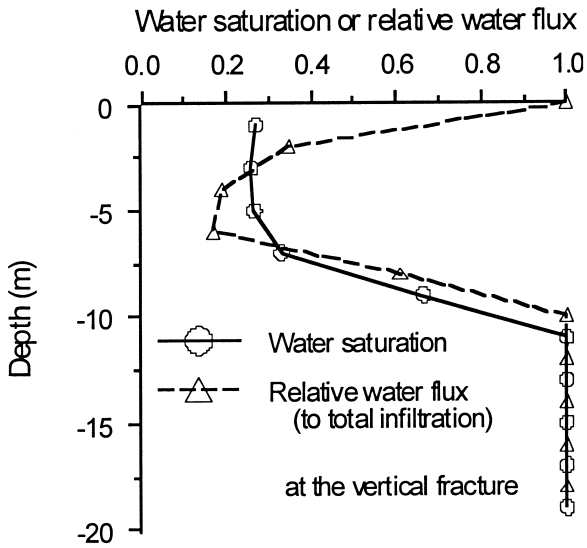

Fig. 8. Steady-state water saturation and relative water flux (to total infiltration) passed through the fractures.

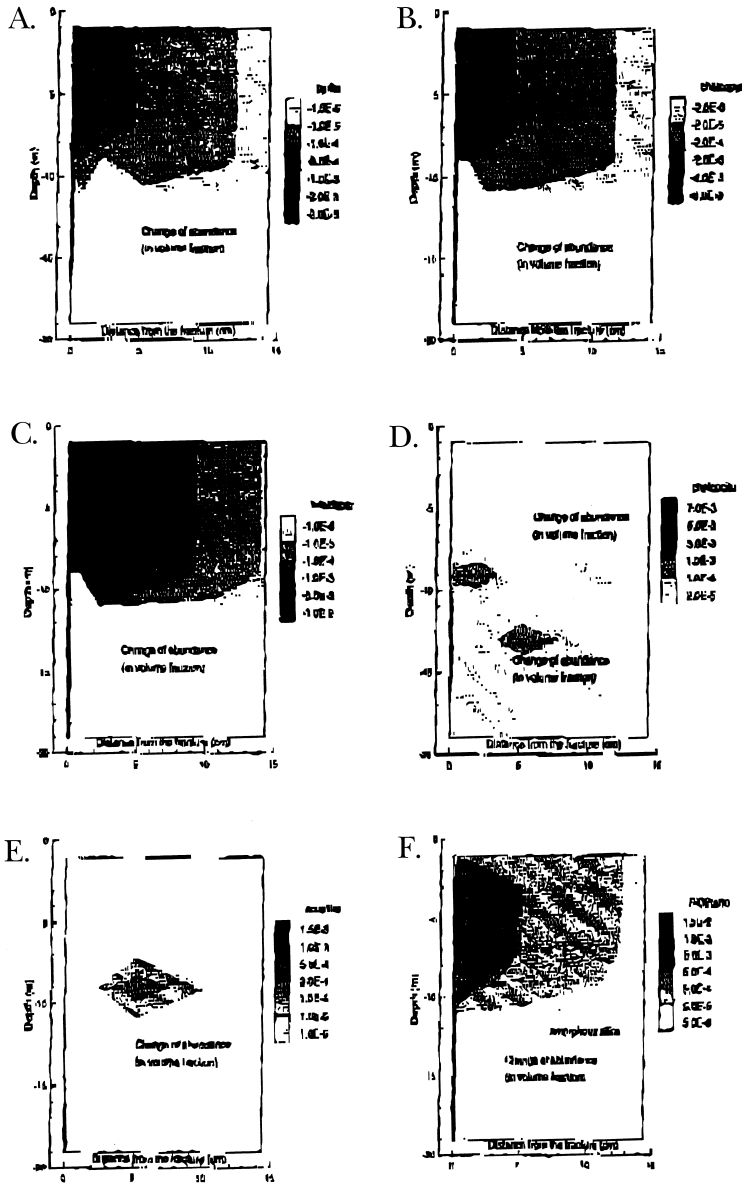

Fig. 9. Change of mineral abundance (positive values indicate precipitation and negative dissolution) after 20,000 yrs in the fractured rock.

infiltration over 5 m depth (fig. 8). Then the water taken up by the matrix is released to the fractures just above the water table (at $z = -10$ m). In the saturated zone, almost all water flows through the fractures since the saturated permeability of the fractures is four orders of magnitude greater than that of the matrix.

Pyrite and chalcopyrite oxidative dissolution takes place mostly in close proximity to the unsaturated fracture zone (fig. 9A and B). Away from the fracture zone, dissolution rates decrease due to limited oxygen access and the reduced reactive

surface areas. The oxygen is supplied to the rock matrix partly advectively, dissolved in water, and partly by aqueous and gaseous diffusion. Oxidative dissolution is seen also to occur in the top part of the saturated fracture zone, which is different from the previous homogeneous porous medium case. This occurs because much higher water flux passes through the saturated fractures, so that much more aqueous oxygen is available, and the oxidizing zone extends locally below the water table. The pH is low in the unsaturated fractures and matrix (fig. 10A).The secondary mineral assemblages take on a more complex pattern than in the 1-D porous medium case. Chalcocite precipitation occurs mostly in the fracture just below the water table (fig. 9D), but some also occurs in the matrix just above as well as below the water table. Although changes in mineral abundance are smaller in the matrix, the volume throughout which these changes occur is considerably larger than in the fractures, so that in terms of overall mineral inventory matrix dissolution and precipitation could be very significant. Most covellite precipitates in the deep fracture below the chalcocite precipitation peak (fig. 9E), and a minor amount precipitates in the matrix just above the water table. Most amorphous silica precipitation occurs in the fractures (fig. 9F). The aqueous and gaseous diffusion processes play an important role in the formation of secondary minerals in the matrix. The small aqueous diffusion coefficient is still significant because water advection is slow with an infiltration rate of 0.015 m yr^{-1}.

The MINC method employed not only enables us to resolve the flow and chemical transport in the matrix block but also to resolve the reactivity of fluid-rock interactions by considering spatially non-uniform reactive surface areas. The study of this fractured rock provides a more detailed picture of supergene copper enrichment (SCE) processes on a smaller scale, while the homogeneous porous medium study gives a general pattern of the SCE on a large scale.

The alteration of the primary minerals and development of secondary mineral assemblages simulated by our model agree with observations in supergene copper deposits (Ague and Brimhall, 1989). The simulation results are consistent in general with known mineral sequences and spatial and temporal patterns observed in nature. De-stabilization of primary sulfide (pyrite and chalcopyrite) is what drives supergene enrichment. Both these minerals were found to dissolve in the simulation. Similarly, the wall rock mineral buffer assemblages that resist changes in solution composition were destroyed. Most

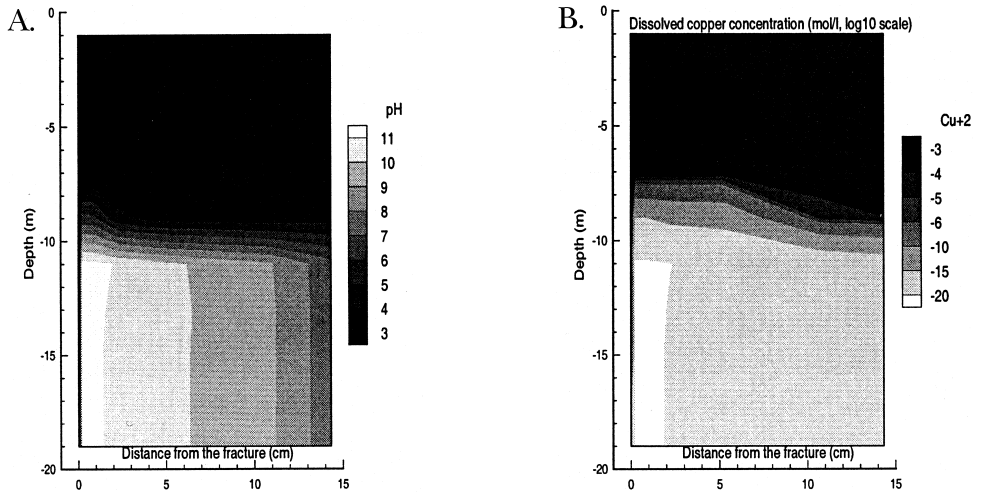

Fig. 10. pH and dissolved copper concentration at 20,000 yrs in the fractured rock.

importantly, the redox buffer (annite-magnetite-orthoclase) was destroyed, thereby allowing the unsaturated part of the systems to oxidize as sulfides were de-stabilized.

It has long been recognized that supergene enrichment is due not to a single stand of the paleo-ground water table but rather to a long-term process of downward accumulation of metals (Locke, 1926) over geological time periods as progressively lower positions within the protore are subjected to oxidation. Enrichment is accomplished by many stages of ground water table descent through a paleo-hydrological evolution (Alpers and Brimhall, 1989), enhanced in certain regions of the Earth by climatic change to more arid conditions (Alpers and Brimhall, 1988). Ultimately, where hyperarid conditions eventually occur, such as in the Atacama desert of Chile, insufficient water is available for supergene processes to proceed and enrichment ceases. Similarly with less rainfall, the erosion rate also declines, and ideal conditions for preservation of enriched ore deposits are attained. Our model results, though drastically simplified compared to these effects of nature, do in fact show that with lowering of the ground water table, the leached zone advances downward and previously-precipitated chalcocite and covellite are leached with their constituent copper ions contributing to the development of a lower stand of the enrichment blanket. In addition, the simulation results suggest the migration rate of the enrichment blanket decreases gradually with depth.

EFFECTS OF THERMOHYDROLOGY ON GEOCHEMISTRY

Problem statement.—The effects of thermohydrology on geochemistry are investigated for the Drift Scale Test (DST) problem, in which a strong heat source is emplaced in unsaturated fractured volcanic tuffs at Yucca Mountain, Nevada (Sonnenthal and others, 1998). The DST test was designed to gain a better understanding of the coupled thermal, hydrological, chemical, and mechanical (THCM) processes that may take place around a heat-generating high-level nuclear waste repository. The test essentially consists of heating up the host rock (a welded tuff) through electric heaters located along a main 50-m drift and through a series of wing heaters. Many THCM parameters are monitored during this test. Details on test design can be found in Birkholzer and Tsang (1997). Here we report on a pre-test analysis of possible mineral alteration and changes in pore-water and gas chemistry that could occur during the heater test.

Understanding the complex interplay of the thermal, hydrological, and chemical processes in the unsaturated fractured welded tuff involves a number of challenges and difficulties: (1) the large permeability contrast between the matrix of the welded tuff (approx 10^{-17} m^2) and the fracture system (10^{-13} m^2); (2) considerable differences in mineralogy such as calcite, opal, and zeolites abundant in fractures but much less common in the matrix; (3) significant changes in thermodynamic and kinetic data with temperature; (4) boiling and condensation phenomena; and (5) a chemically active gas phase.

Problem setup and parameters.—To resolve the disparity in transport processes and mineralogy between the fractures and matrix, we use the dual permeability approach (DK) for the fractured rock. The DK has been described in Xu and Pruess (this issue, p. 16–33). Although this approach has a limited ability to resolve gradients of temperature, water saturation, and chemical concentrations at the fracture-matrix interface, it is a substantial improvement over single continuum or equivalent continuum methods for the fractured tuff. The DK provides a framework that can capture the essential differences in physical and chemical properties between rock matrix and fractures. Although a more refined MINC approach can better resolve the gradients of variables, it has larger computational requirements due to the further detailed discretization of a rock matrix.

For the present study, we employ a two-dimensional vertical cross section based on Birkholzer and Tsang (1997) for a predictive analysis of the thermohydrology. The numerical mesh has 2242 grid blocks for each of the fracture and matrix continua. A close-up view of the mesh around the heated areas is shown in figure 11. Boundary and initial conditions and thermohydrologic properties of the welded tuffs were taken

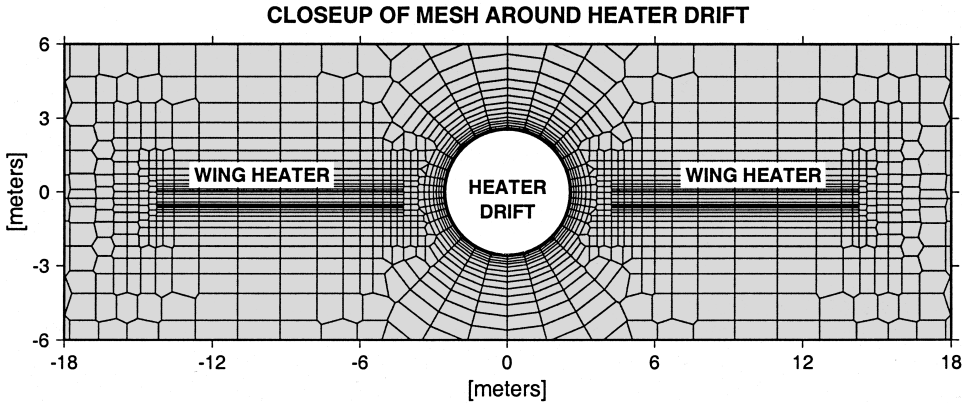

Fig. 11. Closeup view of region around central drift heater and wing heaters showing local grid refinement adopted from Birkholzer and Tsang (1997).

from Birkholzer and Tsang (1997). The chemical evolution is mainly controlled by temperature change. The effect of infiltration on chemical evolution can be neglected, because it is very small (on the orders of a few millimeters per year). The inside wall of the heater drift is considered to be a no-flux boundary for water, vapor, and aqueous and gaseous species. The initial water composition used in the simulation is presented in table 6. The interaction of CO_2 gas with the aqueous solution is assumed at equilibrium. Initial mineral volume fractions, possible secondary mineral phases considered, and reaction rate law parameters are presented in table 7. Thermodynamic data used in the simulations were taken from the EQ3/6 V7.2b database (Wolery, 1992); these were derived using SUPCRT92 (Johnson, Oelkers, and Helgeson, 1992). Full details on problem setup and parameters for this coupled simulation of thermo-hydro-chemical processes can be found in Sonnenthal and others (1998).

TABLE 6

Initial pore and fracture water composition used in the simulation for The Drift-Scale-Heater Test at Yucca Mountain, Nevada (Sonnenthal and others, 1998). These values are average of water sample data from wells UZ-16, SD-9 and SD-12 (Yang and others, 1996)

Component	Concentration (mg/L)
Ca^{2+}	27
Mg^{2+}	5
Na^{+}	91
HCO_3^{-}	219*
Cl^{-}	41
SO_4^{2-}	40
SiO_2	60
Al	1×10^{-6} **
K	4**
pH	8.2

* Adjusted for charge balance

** Estimated

TABLE 7

Initial mineral volume fractions (V_f) and possible secondary mineral phases ($V_f = 0.0$) considered in the simulation. The kinetic rate law used is given in eq (1) of Xu and Pruess (this issue, p. 16–33), with the parameters μ and n set equal to one (first order kinetics). The rate constant k is calculated from eq (2) using kinetic constants at 25 °C (k_{25}) and activation energy (E_a). Parameters k_{25} and E_a are calculated from Johnson and others (1998), Hardin (1998), and Tester and others (1994) or estimated from these data. Calcite and anhydrite are considered equilibrium minerals. Precipitation rate law for amorphous silica used is from Rimstidt and Barnes (1980), log k = −7.07 −2598/T(K). All other kinetic minerals were given the same rate law for precipitation as dissolution, except quartz and cristobalite for which precipitation was suppressed

Minerals	V_f (matrix)	V_f (fractures)	k_{25} (mol/m^{2}s)	E_a (kJ/mol)	Surface area (m^2/kgH_2O)
Quartz	0.1018	0.0995	1.2589×10^{-14}	87.5	71.07
Cristobalite-a	0.2292	0.2241	3.1623×10^{-13}	69.08	71.07
Amorphous silica	0.0	0.0	7.944×10^{-13}	62.8	142.14
Calcite	0.0	0.02	at equilibrium		
Anhydrite	0.0	0.0	at equilibrium		
Microcline	0.3009	0.2942	1.0×10^{-12}	57.78	142.4
Albite-low	0.2498	0.2441	1.0×10^{-12}	67.83	104.2
Anorthite	0.0083	0.0087	1.0×10^{-12}	67.83	124.6
Kaolinite	0.0	0.0	1.0×10^{-13}	62.80	142.4
Illite	0.0	0.005	1.0×10^{-14}	58.62	142.4
Sepiolite	0.0	0.0	1.0×10^{-14}	58.62	142.4
Smectite-Na	0.0	0.0	1.0×10^{-14}	58.62	142.4
Smectite-K	0.0	0.0	1.0×10^{-14}	58.62	142.4
Smectite-Ca	0.0	0.0	1.0×10^{-14}	58.62	142.4
Smectite-Mg	0.0	0.0	1.0×10^{-14}	58.62	142.4

Results.—To facilitate the analysis, we present graphs showing parameter variations along the vertical profile of the wing heater at 12 m to the left of the heater drift (see fig. 11). These graphs are complemented with contour plots of some variables to give a general picture. During the initial heating stage, rocks are heated to the boiling point, and evaporation and boiling of pore waters takes place. Boiling occurs primarily in the matrix with vapor discharge into the fractures, and condensation in cooler portions of the fractures. The area closest to the heat source eventually dries up, giving rise to a dryout zone, which is surrounded by a boiling zone (fig. 12). A condensation halo develops around the boiling zones. The condensation leads to liquid saturation increase and subsequent drainage in fractures, mostly toward areas below the heat source (left side of fig. 12). The partial pressures of CO_2 in the fractures are extremely low in the dryout zone because of dilution from sustained boiling (fig. 13). The CO_2 gas diffusion can affect the magnitude of this reduction in the partial pressure. However, sensitivity studies using diffusivities from a maximum value of 1×10^{-5} m^2/s to zero have shown that values of the partial pressure always decrease, yet to a somewhat lesser degree when larger diffusivities are used. Fracture pore water pH is shifted to high values, near 10 in the condensation zone and extreme values above 11 in the dryout/boiling zone (figs. 12C and 14). The pH increase results from CO_2 degassing:

$$HCO_3^- + H^+ \rightarrow CO_2(g) + H_2O \qquad (1)$$

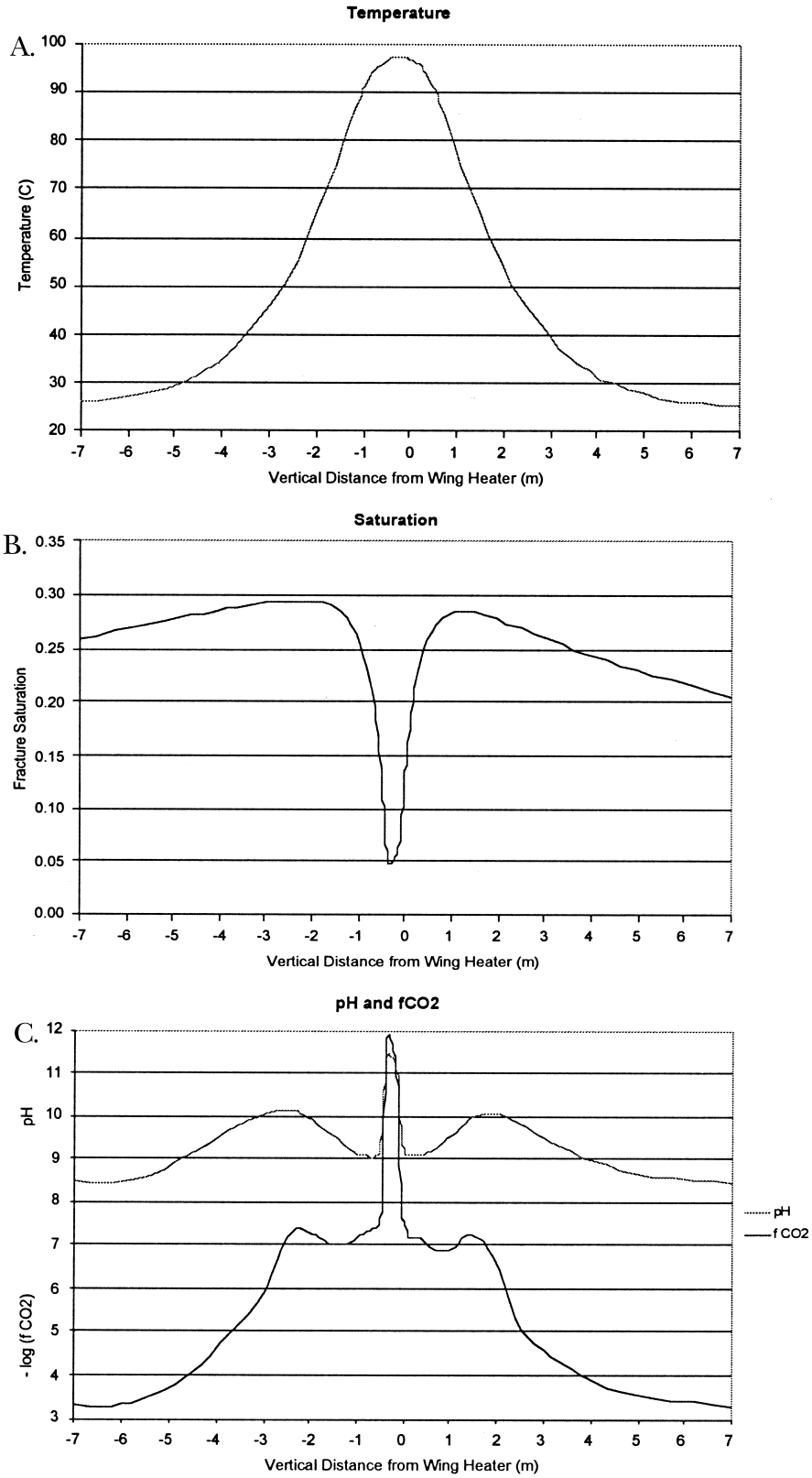

Fig. 12. Temperature (A), liquid saturation (B), and pH and CO_2 gas partial pressure (C) for the fractures along a vertical profile through the wing heater after two months (at 12 m, see fig 11; Positive distance values indicate elevations above the heater, negative below).

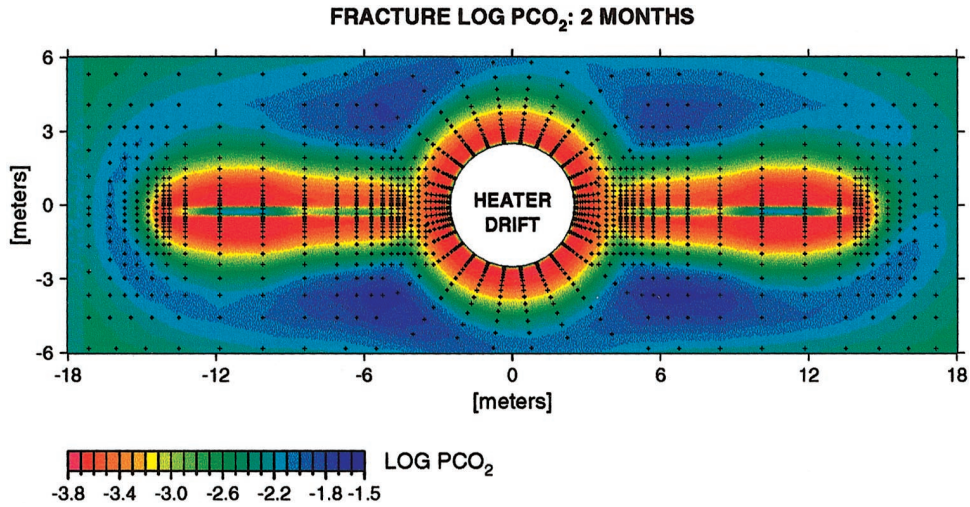

Fig. 13. Contour plot of CO_2 gas partial pressure in fractures after two months of heating.

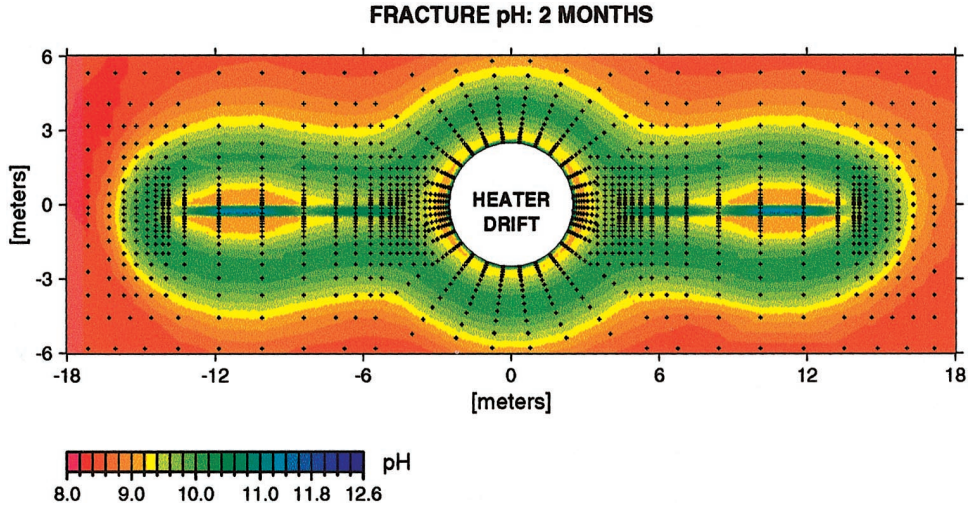

Fig. 14. Contour plot of pore water pH in fractures after two months of heating.

This pH increase together with the temperature increase leads to precipitation of calcite (fig. 15), whose solubility decreases with temperature,

$$Ca^{2+} + HCO_3^- \rightarrow CaCO_3 \text{ (calcite)} + H^+ \quad (2)$$

The pH changes are accompanied by other mineral-water interactions such as the conversion between anorthite and kaolinite with calcite precipitation:

$$CaAl_2Si_2O_8 \text{ (anorthite)} + H_2O + HCO_3^- + H^+ \rightarrow$$
$$Al_2Si_2O_5(OH)_4 \text{ (kaolinite)} + CaCO_3 \text{ (calcite)} \quad (3)$$

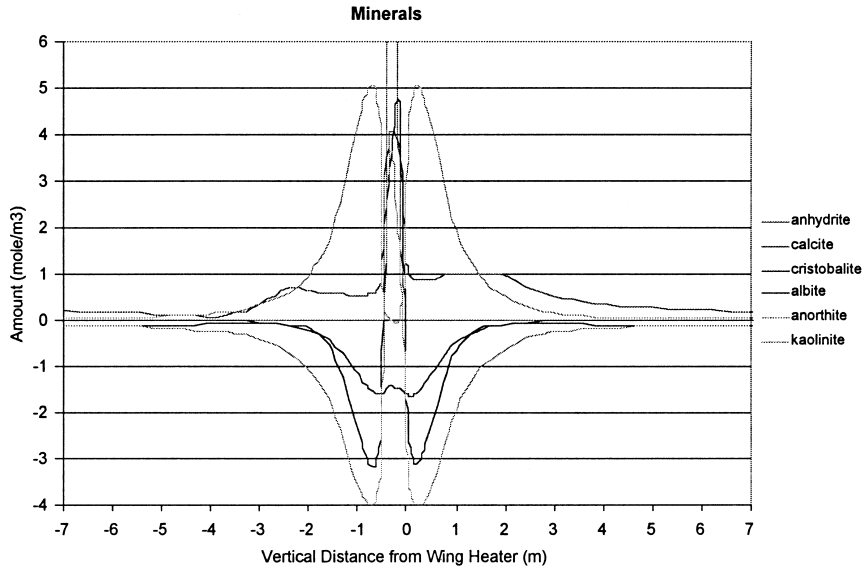

Fig. 15. Change of mineral abundance in fractures along the vertical profile (positive for precipitation and negative for dissolution) after two months of heating.

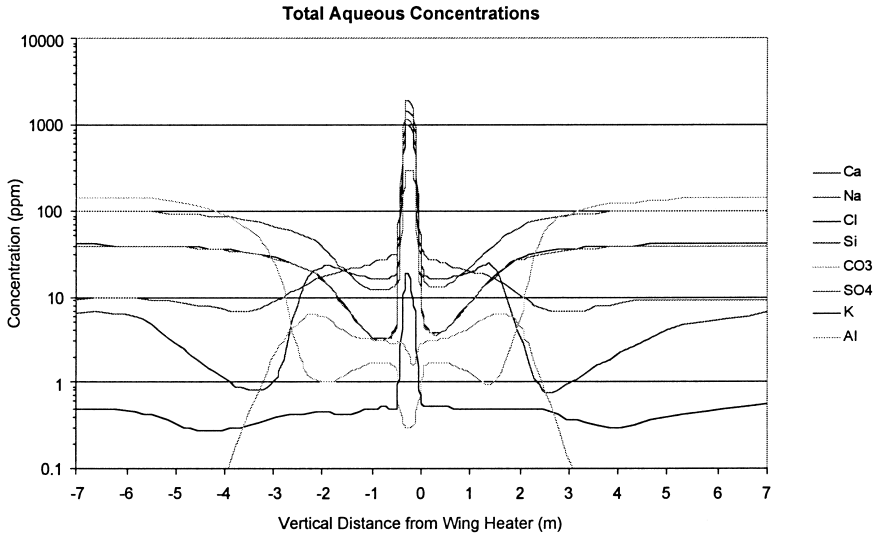

Fig. 16. Aqueous chemical concentration in fractures along the vertical profile after two months of heating.

From figure 15, we can see a clear correspondence between anorthite dissolution and kaolinite precipitation as the temperature increases, especially in the two condensation zones.

At about 3 m from the heater, the total aqueous carbonate concentration (fig. 16) starts to drop significantly due to CO_2 degassing and calcite precipitation. At 2 m from the heater, the decreasing trends of chloride, sulfate, and sodium clearly indicate

dilution from vapor condensation. This condensation is accompanied by CO_2 dissolution, resulting in pH dropping more than 1 unit from the boiling zone (fig. 12C). The position of two local pH minima at the condensation zones is consistent with the local minimum of chloride, sulfate, and sodium concentrations caused by vapor condensation. The lower pH further drives reaction (3) and precipitates kaolinite from dissolution of anorthite as well as of albite (fig. 15):

$$2NaAlSi_3O_8 \text{ (albite)} + H_2O + 2H^+ \rightarrow$$
$$Al_2Si_2O_5(OH)_4 \text{ (kaolinite)} + 4SiO_2(aq) + 2Na^+ \quad (4)$$

Again the local maximum of kaolinite abundance and minimum of anorthite and albite abundances are consistent with the pH local minimum (at condensation zones).

In the boiling zone, a sharp reversal of reactions (3) and (4) can be observed (fig. 15) due to degassing and pH increase. The cristobalite dissolution (fig. 15) is mainly controlled by temperature and is not sensitive to changes in CO_2 partial pressure and pH. The general pictures of changes in cristobalite and kaolinite volume fraction due to dissolution and precipitation in fractures are presented in figures 17 and 18, respectively.

Changes in CO_2 partial pressure in this fractured rock system play a very important role in pH and water chemistry and subsequent mineral alteration. The patterns of mineral dissolution and precipitation in the boiling zone (precipitation dominant except for cristobalite) is completely different from those in the condensation zone due to different CO_2 liquid-gas partitioning behavior (degassing in the boiling zone and dissolution in the condensation zone). The simulated calcite precipitation in the high temperature fracture region agrees with field observations from hydrothermal systems such as Long Valley Caldera, California (White and Peterson, 1991).

Because of numerous uncertainties, the preliminary modeling results should not be used to infer the long-term behavior of a nuclear waste repository. For example, the kinetics of heterogeneous reactions are scale and history-dependent and cannot be reliably quantified. Reactive surface areas are uncertain and subject to poorly quantifi-

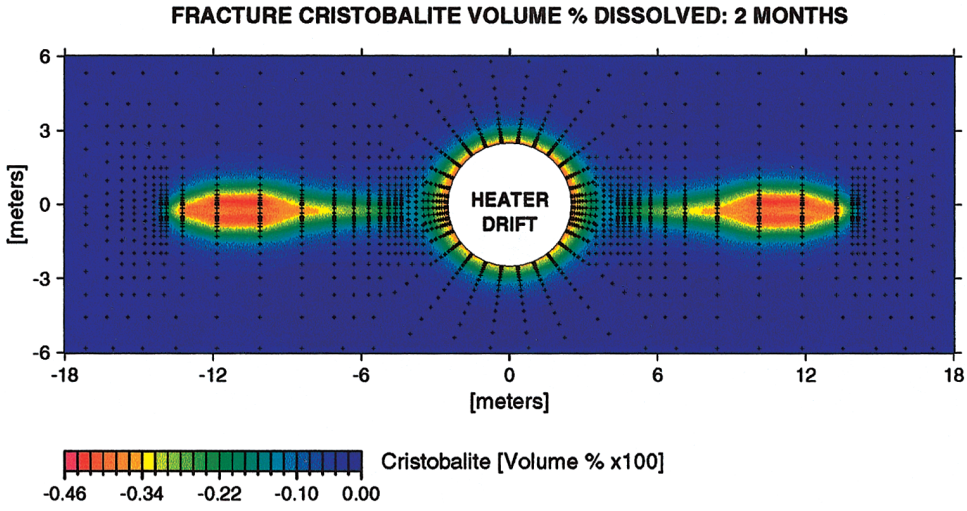

Fig. 17. Contour plot of change of cristobalite abundance (in volume percentage) in fractures after two months of heating.

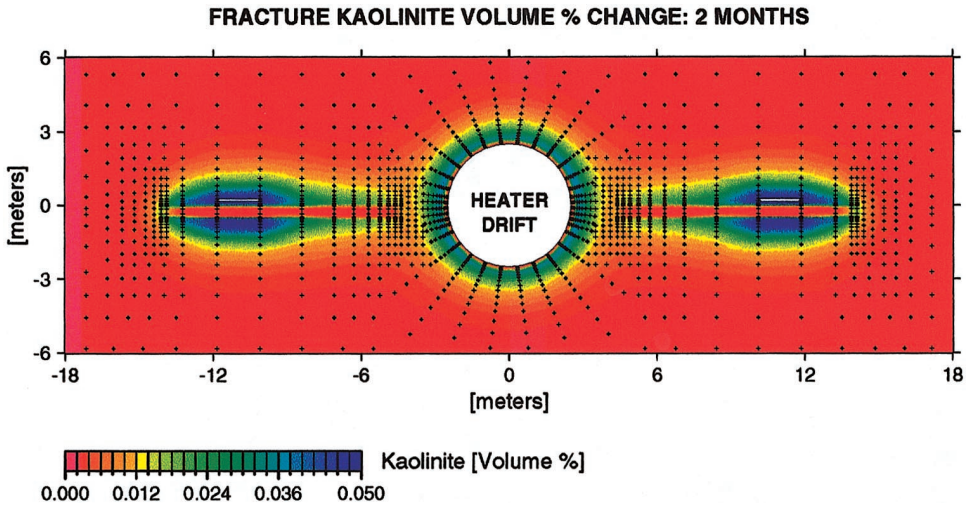

Fig. 18. Contour plot of change of kaolinite abundance (in volume percentage) in fractures after two months of heating.

able phenomena such as armoring of mineral phases by others. Two-phase flow in fractured rock is affected by multi-scale heterogeneities. The enormous intrinsic variability of two-phase flow in fractures severely limits possibilities for a fully mechanistic description (Kneafsey and Pruess, 1998). The "numerical experiments" give a detailed albeit approximate view of the dynamical interplay between coupled hydrologic, thermal, and chemical processes and can provide useful insight into process mechanisms such as fracture-matrix interaction, liquid-gas phase partitioning, and conditions and parameters controlling mineral alteration.

DISCUSSION

Gas effects.—The two modeling studies have demonstrated that the presence of a gas phase in unsaturated geologic media has strong influences on hydrogeochemical evolution. In supergene enrichment systems, the oxygen consumed during pyrite and chalcopyrite oxidation is mainly supplied by diffusive transport in the gas-filled portion of the pore space from the land surface boundary. As a result of strongly acidic conditions, the primary minerals in the unsaturated zones are intensely altered and metal ions are transported downward. The gaseous oxygen availability depends mainly on the depth from the land surface, the gas phase saturation, and the medium porosity and tortuosity. Gaseous oxygen can not be accessed in the saturated zone, and transport of aqueous oxygen in liquid phase is slow and limited due to low solubility and infiltration rate. Oxidation of pyrite and chalcopyrite generally only takes place at the top of the saturated zone but in a fractured medium can occur below the water table where oxygen dissolved in infiltrating water is available in the fractures. Oxidation rates in regions with large water saturation (rock matrix and below the water table) are limited by oxygen availability, not by chemical kinetics.

In the artificial hydrothermal system created by emplacing a strong heat source into unsaturated tuffs at Yucca Mountain, the CO_2 gas partial pressure plays a crucial role in controlling the system pH, pore water chemistry, and then mineral dissolution and precipitation patterns. CO_2 degassing due to the temperature increase results in pH increase. This pH increase, together with the temperature increase, leads to the precipitation of calcite. The different patterns of change in pH between the boiling

and condensation zones (resulting from different CO_2 liquid-gas partitioning behavior) cause different patterns of mineral dissolution and precipitation such as precipitation of anorthite and albite in the boiling zone and dissolution of these minerals in the condensation zone.

Fractured rock.—Geochemical transport behavior in fractured rocks is different from that in porous media. As demonstrated in the supergene enrichment system, physical heterogeneity (permeability contrast between fracture and matrix) results in the heterogeneous localized distribution of secondary ore deposits. Jointed rocks show relatively unaltered cores surrounded by intensely altered rocks closer to the fractures where chemical weathering has proceeded (Brimhall and Dietrich, 1987). For unsaturated fractured rocks with low matrix permeability, strong capillary suction effects from the small matrix pores draw water away from the fractures, whose pore space is mostly occupied by gas phase. Oxygen in the unsaturated fractures is dominantly transported through gas diffusion, while it is supplied to the unsaturated matrix partly by gas transport and partly by aqueous transport. Mineral composition of the rock matrix may be considerably different from that of the fractures, resulting in different geochemical transport behavior between the matrix and fractures. Multiple continuum approaches allow to resolve flow and chemical transport in fractures and matrix blocks and to account for differences in reactivity of fluid-rock interaction due to dependence of mineral abundance and reactive surface area on distance from the fractures. These approaches can capture the essential physical and chemical heterogeneity of fractured rocks.

In the heater test, the large permeability contrast between the matrix and the fracture system results in extremely different liquid and vapor flow in the two media. Boiling occurs primarily in the matrix with water vapor discharge into the fractures and condensation in cooler portions of the fractures followed by water imbibition into the matrix. As a result, the partial pressures of CO_2 in the fractures are extremely low (on the order of 10^{-12}-10^{-11} bar) in the boiling zone because of degassing. Some CO_2 accumulates in the cooler condensation zones where partial pressure reaches about 10^{-7} bar. Changes in CO_2 partial pressure in this fractured rock system control pH and subsequent mineral alteration patterns. For example, anorthite and albite precipitate in the boiling zone, whereas these minerals dissolve in the condensation zones.

Heat effects.—In the heater test, chemical evolution is driven mainly by temperature increase. Fluid flow and geochemical behavior are affected by temperature dependence of (1) water and CO_2 partitioning between liquid and gas phases, (2) thermophysical properties such as fluid density, viscosity, and gas solubility, and (3) chemical properties such as thermodynamic and kinetic constants. Heat-driven vaporizing fluid flow is strongly coupled with gas such as CO_2 geochemistry in unsaturated fracture-matrix system. The heat effects are complicated by fracture-matrix interaction, where CO_2 is discharged into the fractures along with water vapor from boiling regions of the matrix and subsequently accumulates in condensation zones in the fractures. The changes in water saturation, CO_2 partial pressure, pH, water chemistry, and mineral alteration pattern, are all controlled by temperature increase due to heating.

Geochemical batch models.—The traditional approach for analyzing geochemical evolution and rock alteration involves separating fluid flow from chemical transport, using geochemical batch models such as PHREEQE (Parkhurst, Thorstenson, and Plummer, 1980), CHILLER (Reed, 1982), and EQ3/6 (Wolery, 1992). However, the geochemical evolution in fractured rock systems occurs through coupled processes of multi-phase fluid and heat flow and chemical transport. For the supergene enrichment problem, advective and diffusive transport of reactants is essential to account for the simultaneous oxidative weathering in the unsaturated zone and reprecipitation of ore

compounds in the saturated zone just below the water table. In the heater test, heat-driven vaporizing fluid flow is strongly coupled with CO_2 gas geochemistry under two-phase conditions. Mineral alteration patterns are mainly controlled by vaporizing flow and CO_2 liquid-gas phase partitioning in the heterogeneous fracture-matrix system.

CONCLUDING REMARKS

We have used a reactive transport simulation tool TOUGHREACT to investigate: (1) natural supergene copper enrichment in unsaturated-saturated fractured media and (2) geochemical processes in an artificial hydrothermal system created in an anthropogenic drift scale heater test. Through these two examples we have addressed the importance of the following aspects on geochemical evolution: (1) participation of gas phase, (2) fracture-matrix interaction, and (3) heat effects on fluid flow and reaction properties and processes. These three aspects, in a complex coupled fashion, affect geochemical evolution in variably saturated fractured rock.

Numerical simulation of simplified supergene enrichment systems which are hydro-chemically differentiated by the vadose zone can offer confirmation of well-posed questions based upon field study and petrologic information. Specifically, it has been possible here to demonstrate that acidification and oxidation of primary pyrite and chalcopyrite drives supergene leaching and destroys wall rock mineral solution buffer assemblages that otherwise restrain redox conditions to a reducing level. Furthermore, it was shown that with lowering of the ground water table, previously precipitated chalcocite and covellite can be oxidized, and their contained copper remobilized to a lower position of the enrichment blanket. Oxidation rates in regions with large water saturation (rock matrix and below the water table) are limited by oxygen availability, not by chemical kinetics. These results illustrate how by abstraction of a simplified set of relevant factors, certain natural processes can be effectively modeled and how model validity can be tested against qualitative field observations.

In the in-situ heater test, changes in CO_2 partial pressure in the fractured rock system play a very important role in pH, water chemistry, and mineral alteration. The simulated calcite precipitation in the high temperature fracture region agrees with field observations from some hydrothermal fields such as Long Valley Caldera, California (White and Peterson, 1991). The example also shows that fracture-matrix interaction, heat-driven vaporizing fluid flow, and CO_2 degassing are important for the geochemical evolution.

The range of problems concerning the interaction of fluids with rocks is very broad. The present simulation results are specific to the conditions and parameters considered and water and gas chemistry used in this study. Care should be taken when extrapolating the results and conclusions for other sites. Our "numerical experiments" give a detailed view of the dynamical interplay between coupled hydrologic, thermal, and chemical processes, albeit in an approximate fashion. The modeling results can provide useful insight into process mechanisms such as fracture-matrix interaction, liquid-gas phase partitioning, and conditions and parameters controlling geochemical evolution.

ACKNOWLEDGMENTS

The authors appreciate stimulating discussions with Frederic Gérard and Tom Wolery. This paper has benefited significantly from suggestions and comments made during the review process by Carl Steefel and an anonymous reviewer. This work was supported by the Laboratory Directed Research and Development Program of the Ernest Orlando Lawrence Berkeley National Laboratory, under Contract No. DE-AC03–76SF00098 with the U.S. Department of Energy; and by the Director, Office of Civilian Radioactive Waste Management, U.S. Department of Energy, through Memorandum

Purchase Order EA9013MC5X between TRW Environmental Systems Inc., and the Ernest Orlando Lawrence Berkeley National Laboratory.

References

Ague, J. J., and Brimhall, G. H., 1989, Geochemical modeling of steady state and chemical reaction during supergene enrichment of porphyry copper deposits: Economic Geology, v. 84, p. 506–528.

Alpers, C. A., and Brimhall, G. H, 1988, Middle Miocene climatic change in the Atacama Desert, northern Chile: Evidence from supergene mineralization at La Escondida: Geological Society of America, v. 100, p.1640–1655.

——— 1989, Paleohydrologic evolution and geochemical dynamics of cumulative supergene metal enrichment at La Escondida, Atacam Desert, Northern Chile: Economic Geology, v. 84, p. 229–255.

Birkholzer, J. T., and Tsang, Y. W., 1997, Pretest analysis of the thermal-hydrological conditions of the ESF Drift Scale Test, Yucca Mountain Project Level 4 Milestone SP9322M4: Berkeley, California, Lawrence Berkeley National Laboratory.

Brimhall, G. H., Alpers, C. N., and Cunningham, A. B., 1985, Analysis of supergene ore-forming processes and ground water solute transport using mass balance principles: Economic Geology, v. 80, p. 1227–1256.

Brimhall, G. H., and Dietrich, W. E., 1987, Constitutive mass balance relations between chemical composition, volume, density, porosity, and strain in metasomatic hydrochemical systems: Results on weathering and pedogenesis: Geochimica et Cosmochimica Acta, v. 51, p. 567–587.

DePaolo, D. J., 1999, Isotopic effects in dual-porosity fluid-rock systems, In: Proceedings of International Symposium on Dynamics of Fluids in Fractured Rocks: Berkeley, California, Lawrence Berkeley National Report LBNL-42718.

Domenico, P. A., and Schwarzt, F. W., 1990, Physical and Chemical Hydrogeology: New York, John Wiley and Sons, 824 p.

Engesgaard, P., and Kipp, K. L., 1992, A geochemical transport model for redox-controlled movement of mineral fronts in groundwater flow systems: A case of nitrate removal by oxidation of pyrite: Water Resources Research, v. 28, p. 2829–2843.

Gérard, F., Xu, T., Brimhall, G., and Pruess, K., 1997, Modeling reactive chemical transport problems with the codes EQ3/6 and TRANQUI: Berkeley, California., Lawrence Berkeley Laboratory Report LBL-40505.

Hardin, E. L., 1998, Near-field/altered zone models, Milestone report for the CRWMS M&O, U. S. Department of Energy, SP3100M4: Livermore, California, Lawrence Livermore National Laboratory.

Johnson J. W., Knauss K. G., Glassley W. E., Deloach L. D., and Tompson, A. F. B., 1998, Reactive transport modeling of plug-flow reactor experiments: Quartz and tuff dissolution at 240°C: Journal of Hydrology, v. 209, p. 81–111.

Johnson, J. W., Oelkers, E. H., and Helgeson, H. C., 1992, SUPCRT92: A software package for calculating the standard molal thermodynamic properties of minerals, gases, aqueous species, and reactions from 1 to 5000 bars and 0 to 1000 degrees C: Computers and Geosciences, v. 18, p. 899–947.

Kneafsey, T. J., and Pruess, K., 1998, Laboratory experiments on heat-driven two-phase flows in natural and artificial rock fractures: Water Resources Research, v. 34, p. 3349–3367.

Lichtner, P. C., 1988, The quasi-stationary state approximation to coupled mass transport and fluid-rock interaction in a porous medium: Geochimica et Cosmochimica Acta, v. 52, p. 143–165.

Locke, A., 1926, Leached outcrops as guides to copper ores: Baltimore, Maryland, Williams Wilkins Co., 166 p.

Mote, T. I, and Brimhall, G. H, 1999, Mass balance analysis of exotic ore-forming processes and lateral copper transport into the drainage networks of the El Salvador porphyry copper deposit, Chile and its application to discovery of the new exotic mineralization in Quebrada Turquesa: Economic Geology, in press.

Nordstrom, D. K., Alpers, C. N., 1997, The Environmental geochemistry of mineral deposits. Part A. Processes, methods and health Issues, *in* Society of Economic Geologists, Plumlee, G. S., Logsdon, M. J., editors: Reviews in Economic Geology, v. 6.

Olson, G. J., 1991, Rate of pyrite bioleaching by *Thiobacillus ferrooxidans* - Results of an interlaboratory comparison: Applied and Environmental Microbiology, v. 57, p. 642–644.

Parkhurst, D. L., Thorstenson, D. C., and Plummer, L. N., 1980, PHREEQE: A computer program for geochemical calculations: US Geological Survey, Water Resources Investigation Report 80–96, 174 p.

Plummer, L. N., Wigley, T. M., and Parkhurst, D. L., 1978, The kinetics of calcite dissolution in CO_2 systems at 5°C to 60°C and 0.0 to 1.0 atm CO_2: American Journal of Science, v. 278, p. 179–216.

Pruess, K., 1999, A mechanistic model for water seepage through thick unsaturated zones in fractured rocks of low matrix permeability: Water Resources Research, v. 35, (4), p. 1039–1051.

Pruess, K., and Narasimhan, T. N., 1985, A practical method for modeling fluid and heat flow in fractured porous media: Society of Petroleum Engineers Journal, v. 25, (1), p. 14–26.

Reed, M. H., 1982, Calculation of multicomponent chemical equilibria and reaction processes in systems involving minerals, gases and aqueous phase: Geochimica et Cosmochimica Acta, v. 46, p. 513–528.

Rimstidt, J. D., and Barnes, H. L., 1980, The kinetics of silica-water reactions: Geochimica et Cosmochimica Acta, v. 44, p. 1683–1699.

Singer, P.C., and Stumm, W., 1970, Acid mine drainage - The rate determining step: Science, v. 167, p. 1121–1123.

Sonnenthal, E., Spycher, N., Apps, J. A., and Simmons, A., 1998, Thermo-hydro-chemical predictive analysis for the drift-scale heater test, Yucca Mountain Project Level 4 Milestone SPY289M4: Berkeley, California, Lawrence Berkeley National Laboratory Report.

Steefel, C. I., and van Cappellen, P., 1990, A new kinetic approach to modeling water-rock interaction: The role of nucleation, precursors and Ostwald ripening: Geochimica et Cosmochimica Acta, v. 54, p. 2657–2677.

Stumm, W., and Morgan, J. J., 1981, Aquatic chemistry: An Introduction Emphasizing Chemical Equilibria in Natural Waters: New York, John Wiley & Sons, 780 p.

Tester, J. W., Worley, W. G., Robinson, B. A., Grigsby, C. O., and Feerer, J. L., 1994, Correlating quartz dissolution kinetics in pure water from 25 to 625°C: Geochimica et Cosmochimica Acta, v. 58, (11), p. 2407–2420.

Thordarson, W., 1965, Perched groundwater in zeolitized-bedded tuff, Rainier Mesa and Vicinity, Nevada Test Site, Nevada: U. S. Geological Survey Report TEI-862, 93 p.

Van Genuchten, M. T., 1980, A closed-form equation for predicting the hydraulic conductivity of unsaturated soils: Soil Science Society of America Journal, v. 44, p. 892–898.

Warren, J. E., and Root, P. J., 1963, The behavior of naturally fractured reservoirs: Society of Petroleum Engineers Journal, Transactions, AIME, v. 228, p. 245–255.

White, A. F., and Peterson, M. L., 1991, Chemical equilibrium and mass balance relationships associated with Long Valley hydrothermal system, California, USA: Journal of Volcanology and Geothermal Research, v. 48, p. 283–302.

Wolery, T. J., 1992, EQ3/6: Software package for geochemical modeling of aqueous systems: Package overview and installation guide (version 7.0): Livermore, California, Lawrence Livermore National Laboratory Report UCRL-MA-110662 PT I.

Xu, T., and Pruess, K., 2001, Modeling multiphase non-isothermal fluid flow and reactive geochemical transport in variably saturated fractured rocks: 1. Methodology: the first one of this two-part paper, American Journal of Science, v. 301, p. 16–33

Xu, T., Pruess, K., and Brimhall, G., 1999, Oxidative weathering chemical migration under variably saturated conditions and supergene copper enrichment: Berkeley, California, Lawrence Berkeley National Laboratory Report LBNL-43129, 41 p.

Yang, I. C., Yu, P. Rattray, G. W., and Thorstenson, D. C., 1996, Interpretations of chemical and isotropic data from boreholes in the unsaturated zone at Yucca Mountain, Nevada: U. S. Geological Survey Water Resources Investigation Report 96–4058, 57 p.